

Analyzing the Fierz rearrangement freedom for local chiral two-nucleon potentials

L. Huth,^{1,2,*} I. Tews,^{3,4,†} J. E. Lynn,^{1,2,‡} and A. Schwenk^{1,2,5,§}

¹*Institut für Kernphysik, Technische Universität Darmstadt, 64289 Darmstadt, Germany*

²*ExtreMe Matter Institute EMMI, GSI Helmholtzzentrum für Schwerionenforschung GmbH, 64291 Darmstadt, Germany*

³*Institute for Nuclear Theory, University of Washington, Seattle, Washington 98195-1550, USA*

⁴*JINA-CEE, Michigan State University, East Lansing, Michigan, 48823, USA*

⁵*Max-Planck-Institut für Kernphysik, Saupfercheckweg 1, 69117 Heidelberg, Germany*

Chiral effective field theory is a framework to derive systematic nuclear interactions. It is based on the symmetries of quantum chromodynamics and includes long-range pion physics explicitly, while shorter-range physics is expanded in a general operator basis. The number of low-energy couplings at a particular order in the expansion can be reduced by exploiting the fact that nucleons are fermions and therefore obey the Pauli exclusion principle. The antisymmetry permits the selection of a subset of the allowed contact operators at a given order. When local regulators are used for these short-range interactions, however, this “Fierz rearrangement freedom” is violated. In this paper, we investigate the impact of this violation at leading order (LO) in the chiral expansion. We construct LO and next-to-leading order (NLO) potentials for all possible LO-operator pairs and study their reproduction of phase shifts, the ⁴He ground-state energy, and the neutron-matter energy at different densities. We demonstrate that the Fierz rearrangement freedom is partially restored at NLO where subleading contact interactions enter. We also discuss implications for local chiral three-nucleon interactions.

I. INTRODUCTION

Chiral effective field theory (EFT) [1, 2] is a powerful framework to derive nuclear interactions. It is connected to the symmetries of quantum chromodynamics (QCD) and provides a systematic expansion for nuclear forces, including two-nucleon (NN) and many-nucleon interactions, which enables calculations with controlled theoretical uncertainties. Chiral EFT explicitly includes long-range pion-exchange physics and parametrizes shorter-range physics by the most general set of contact operators that is permitted by all symmetries of QCD. Thus, in chiral EFT, NN interactions are given by the sum of pionic and short-range contributions,

$$V_{NN}(Q, \Lambda, C_i^{(\pi)}) = V_\pi(Q, \Lambda, C_i^\pi) + V_{\text{cont}}(Q, \Lambda, C_i), \quad (1)$$

where Q denotes the momenta involved or the pion mass and Λ is a regularization or cutoff scale. Furthermore, V_π stands for the contribution to the interaction from long-range pion exchanges, while V_{cont} contains all of the contributions from short-range contact operators. The long-range pion exchanges depend on a set of pion-nucleon couplings, C_i^π , and the short-range interactions depend on a set of low-energy couplings (LECs), C_i , that are typically fit to experimental data. Considerable effort has been invested recently into the improvement of chiral interactions; see, e.g., Refs. [3–7].

The most general set of NN contact operators at a particular order in the chiral expansion is given by all

combinations of spin, isospin, and momentum operators that are permitted by the symmetries at this order. In addition to the spin and isospin of the two nucleons, these operators depend on two momenta that can be chosen to be the momentum transfer $\mathbf{q} = \mathbf{p}' - \mathbf{p}$ with the incoming and outgoing relative momenta $\mathbf{p} = (\mathbf{p}_1 - \mathbf{p}_2)/2$ and $\mathbf{p}' = (\mathbf{p}'_1 - \mathbf{p}'_2)/2$, respectively, and the momentum transfer in the exchange channel $\mathbf{k} = \frac{1}{2}(\mathbf{p}' + \mathbf{p})$. Interactions that depend only on \mathbf{q} are local, i.e., they depend only on the relative distance \mathbf{r} upon Fourier transformation to coordinate space, while \mathbf{k} dependencies lead to nonlocal interactions.

The number of contact operators at each order in the chiral expansion can be reduced (by a factor of two for NN interactions), due to the fact that nucleons are fermions and therefore obey the Pauli exclusion principle. As a result of the antisymmetry, only a subset of the allowed contact operators at a given order is linearly independent. Generally only the linearly independent contact operators are therefore included. While several subsets can be chosen at each order, they all lead to the same predictions for physical observables. This property is known as Fierz rearrangement freedom or Fierz ambiguity, given the analogy to Fierz identities in four-fermion interactions [8].

Recently, local chiral interactions have been developed that can be used in quantum Monte Carlo (QMC) methods [9–13]. This has led to the first investigations of light nuclei and neutron matter using QMC methods in combination with chiral EFT interactions [13–20]. However, it has been found that local regulator functions introduce sizable regulator artifacts in the three-nucleon ($3N$) sector [11, 15, 21]: First, one finds less repulsion from the $3N$ two-pion-exchange interaction than for typical non-local regulators, and second, there is a violation of the Fierz rearrangement freedom for the short-range $3N$ con-

* E-mail: lukashuth@theorie.ikp.physik.tu-darmstadt.de

† E-mail: itews@uw.edu

‡ E-mail: joel.lynn@gmail.com

§ E-mail: schwenk@physik.tu-darmstadt.de

tact interactions, i.e., calculations depend on the choice of the short-range operators; see also Ref. [22]. While it is true that all regulator functions introduce regulator artifacts at finite cutoffs, the effects of the violation of the Fierz ambiguity have been found to be larger than or comparable to other sources of uncertainty, as demonstrated in Refs. [15, 21]. This additional regulator artifact is present for local short-range regulators [11, 23], but not for typical nonlocal short-range regulators used in previously derived nonlocal $3N$ interactions [24, 25].

A similar violation of the Fierz ambiguity due to local regulators also appears in the NN sector. Based on power counting arguments, one would expect these effects to be even larger in the NN than in the $3N$ sector. Thus, it is important to study how physical observables are affected by the violation of the Fierz ambiguity in NN interactions. Moreover, the NN sector provides an ideal testing ground for understanding this additional regulator artifact.

In this paper, we explore the violation of the Fierz ambiguity at leading order (LO) in the NN sector and investigate the effects of this violation on the local coordinate-space interactions of Refs. [9, 10]. We study phase shifts, the ground-state energy of ^4He using the Green's function Monte Carlo (GFMC) method [26], and the energy per particle of neutron matter using the auxiliary-field diffusion Monte Carlo (AFDMC) method [26] for different short-range operator combinations. After investigating this regulator artifact at LO, we show that at next-to-leading order (NLO) the Fierz rearrangement freedom is partially restored and the remaining violation is smaller than typical chiral uncertainty estimates. We emphasize that this effect is not present in nonlocal NN interactions [5–7, 27, 28] or semilocal interactions [3, 4].

This paper is structured as follows. In Sec. II we explain in more detail the Fierz rearrangement freedom and its relation to different regulator choices. In Sec. III we study the consequences of the violation of the Fierz ambiguity for local chiral LO interactions and then investigate “complete” LO interactions in Sec. IV. In Sec. V we study the effects of the inclusion of NLO corrections. Finally, we summarize in Sec. VI.

II. FIERZ REARRANGEMENT FREEDOM

The NN interaction at LO (Q^0) in Weinberg power counting has two contributions: The local one-pion-exchange (OPE) interaction and momentum-independent contact interactions. The general set of LO contact interactions consistent with the symmetries is given by the spin-isospin operators $\mathbb{1}$, $\sigma_{12} = \boldsymbol{\sigma}_1 \cdot \boldsymbol{\sigma}_2$, $\tau_{12} = \boldsymbol{\tau}_1 \cdot \boldsymbol{\tau}_2$, and $\sigma_{12}\tau_{12}$.

$$V_{\text{cont}}^{(0)} = C_{\mathbb{1}} + C_{\sigma}\sigma_{12} + C_{\tau}\tau_{12} + C_{\sigma\tau}\sigma_{12}\tau_{12}. \quad (2)$$

Even though antisymmetry is a basic symmetry only of the many-body states, in the following we study the an-

tisymmetrized potential to explain the origin of the Fierz rearrangement freedom. The interaction after antisymmetrization, V_{as} , is given by

$$V_{\text{as}}(\mathbf{q}, \mathbf{k}) = \frac{1}{2} (V(\mathbf{q}, \mathbf{k}) - \mathcal{A}[V(\mathbf{q}, \mathbf{k})]), \quad (3)$$

with the antisymmetrizer \mathcal{A} defined via

$$\begin{aligned} \mathcal{A}[V(\mathbf{q}, \mathbf{k})] &= \frac{1}{4}(1 + \sigma_{12})(1 + \tau_{12}) \\ &\times V\left(\mathbf{q} \rightarrow -2\mathbf{k}, \mathbf{k} \rightarrow -\frac{1}{2}\mathbf{q}\right). \end{aligned} \quad (4)$$

Performing the antisymmetrization for the LO contact interaction explicitly, we find [10]

$$\begin{aligned} V_{\text{cont,as}}^{(0)} &= \frac{1}{2} \left(1 - \frac{1}{4}(1 + \sigma_{12})(1 + \tau_{12})\right) V_{\text{cont}}^{(0)} \\ &= \left(\frac{3}{8}C_{\mathbb{1}} - \frac{3}{8}C_{\sigma} - \frac{3}{8}C_{\tau} - \frac{9}{8}C_{\sigma\tau}\right) \mathbb{1} \\ &\quad + \left(-\frac{1}{8}C_{\mathbb{1}} + \frac{5}{8}C_{\sigma} - \frac{3}{8}C_{\tau} + \frac{3}{8}C_{\sigma\tau}\right) \sigma_{12} \\ &\quad + \left(-\frac{1}{8}C_{\mathbb{1}} - \frac{3}{8}C_{\sigma} + \frac{5}{8}C_{\tau} + \frac{3}{8}C_{\sigma\tau}\right) \tau_{12} \\ &\quad + \left(-\frac{1}{8}C_{\mathbb{1}} + \frac{1}{8}C_{\sigma} + \frac{1}{8}C_{\tau} + \frac{3}{8}C_{\sigma\tau}\right) \sigma_{12}\tau_{12} \\ &= \tilde{C}_S + \tilde{C}_T\sigma_{12} + \left(-\frac{2}{3}\tilde{C}_S - \tilde{C}_T\right) \tau_{12} \\ &\quad + \left(-\frac{1}{3}\tilde{C}_S\right) \sigma_{12}\tau_{12}. \end{aligned} \quad (5)$$

As can be seen, there are only two independent couplings at LO after antisymmetrization, and these two couplings contribute to the two possible S -wave scattering channels. Thus, only two out of the four operator structures are necessary to describe the contact physics at LO while the remaining operator structures are recovered after antisymmetrization. In principle, any linearly independent combination of two out of the four contact interactions can be chosen, which is used to reduce the number of LECs when constructing chiral NN interactions.

Chiral EFT is a low-momentum theory and, thus, when using chiral interactions in few- and many-body calculations, it is necessary to apply momentum-dependent regulator functions to cut off high-momentum modes that would otherwise lead to divergences. In general, the regulator function can depend on both momentum scales, $f_R(\mathbf{q}, \mathbf{k})$. Let us now consider the preceding argument with a regulator for the short-range potential included. The Fierz ambiguity is preserved if the regulator commutes with the antisymmetrizer, i.e., when

$$f_R(\mathbf{q}, \mathbf{k}) = f_R\left(-2\mathbf{k}, -\frac{1}{2}\mathbf{q}\right). \quad (6)$$

In this case the regulator is just a prefactor in Eqs. (3) and (5) and does not affect the antisymmetrization procedure: There are still only two independent contact operators at LO. The condition Eq. (6) is fulfilled only when the regulator is a symmetric and even function of \mathbf{q} and $2\mathbf{k}$. This is equivalent to regulating the short-range contact interactions with symmetric and even functions of \mathbf{p} and \mathbf{p}' , as has been done for previously derived nonlocal [5–7, 27, 28] and semilocal interactions [3, 4], which

use the functional form

$$f_R(\mathbf{p}, \mathbf{p}') = \exp \left[- \left(\frac{\mathbf{p}}{\Lambda} \right)^{2n} \right] \exp \left[- \left(\frac{\mathbf{p}'}{\Lambda} \right)^{2n} \right], \quad (7)$$

where n takes integer values.

In contrast, local regulators $f_R(\mathbf{q})$ violate the Fierz rearrangement freedom, because they do not commute with the antisymmetrizer. Introducing the momentum exchange operator \mathcal{P}^m , where $\mathcal{P}^m f(\mathbf{q}, \mathbf{k}) = f(-2\mathbf{k}, -\frac{1}{2}\mathbf{q})$, the antisymmetrized interaction with local regulators is given by

$$\begin{aligned} V_{\text{cont,as}}^{(0,\text{loc})} &= \frac{1}{2} \left(1 - \frac{\mathcal{P}^m}{4} (1 + \sigma_{12})(1 + \tau_{12}) \right) V_{\text{cont}}^{(0)} f_R(\mathbf{q}) \\ &= \mathbb{1} \left(\frac{C_1}{2} f_R(\mathbf{q}) - \frac{1}{8} (C_1 + 3C_\sigma + 3C_\tau + 9C_{\sigma\tau}) f_R(2\mathbf{k}) \right) + \sigma_{12} \left(\frac{C_\sigma}{2} f_R(\mathbf{q}) - \frac{1}{8} (C_1 - C_\sigma + 3C_\tau - 3C_{\sigma\tau}) f_R(2\mathbf{k}) \right) \\ &+ \tau_{12} \left(\frac{C_\tau}{2} f_R(\mathbf{q}) - \frac{1}{8} (C_1 + 3C_\sigma - C_\tau - 3C_{\sigma\tau}) f_R(2\mathbf{k}) \right) + \sigma_{12}\tau_{12} \left(\frac{C_{\sigma\tau}}{2} f_R(\mathbf{q}) - \frac{1}{8} (C_1 - C_\sigma - C_\tau + C_{\sigma\tau}) f_R(2\mathbf{k}) \right), \end{aligned} \quad (8)$$

where $f_R(\mathbf{q}) \neq f_R(2\mathbf{k})$. All of the above combinations of LECs are linearly independent and, thus, the Fierz rearrangement freedom is violated. This violation of the Fierz ambiguity is a manifestation of the fact that introducing a regulator function affects terms beyond the order at which one is working, and should be corrected when subleading contact operators are included. Here we illustrate this explicitly by using a Gaussian local regulator, $f_R(\mathbf{q}) = \exp(-(q/\Lambda)^2)$, such that $\mathcal{P}^m f_R(\mathbf{q}) = f_R(2\mathbf{k}) = \exp(-(k/\Lambda)^2)$. Expressing \mathbf{k} in terms of \mathbf{q} , \mathbf{p} , and \mathbf{p}' , we can write

$$\begin{aligned} \mathcal{P}^m f_R(\mathbf{q}) &= \exp \left(-\frac{q^2}{\Lambda^2} \right) \exp \left(-\frac{4\mathbf{p} \cdot \mathbf{p}'}{\Lambda^2} \right) \\ &= f_R(\mathbf{q}) \left(1 - \frac{4\mathbf{p} \cdot \mathbf{p}'}{\Lambda^2} + \mathcal{O}((Q/\Lambda)^4) \right). \end{aligned} \quad (9)$$

Inserting Eq. (9) into Eq. (8), we find

$$\begin{aligned} V_{\text{cont,as}}^{(0,\text{loc})} &= \left(\tilde{C}_S + \tilde{C}_T \sigma_{12} + \left(-\frac{2}{3} \tilde{C}_S - \tilde{C}_T \right) \tau_{12} \right. \\ &\quad \left. + \left(-\frac{1}{3} \tilde{C}_S \right) \sigma_{12} \tau_{12} \right) f_R(\mathbf{q}) + V_{\text{corr}}^f(\mathbf{p} \cdot \mathbf{p}'), \end{aligned} \quad (10)$$

where $V_{\text{corr}}^f(\mathbf{p} \cdot \mathbf{p}')$ captures the higher-order effects $\sim 4\mathbf{p} \cdot \mathbf{p}'/\Lambda^2 + \mathcal{O}((Q/\Lambda)^4)$ in Eq. (9). Reexpressing \mathbf{p} and \mathbf{p}' in terms of \mathbf{q} and \mathbf{k} , the first correction term in Eq. (9) can be rewritten as

$$-\frac{4\mathbf{p} \cdot \mathbf{p}'}{\Lambda^2} = -\frac{4}{\Lambda^2} k^2 + \frac{1}{\Lambda^2} q^2. \quad (11)$$

These operators will be introduced at NLO in chiral EFT, and, analogously, the higher-order corrections

$\mathcal{O}((Q/\Lambda)^4)$ will be included at next-to-next-to-next-to-leading order (N^3LO) and beyond.

The higher-order terms $V_{\text{corr}}^f(\mathbf{p} \cdot \mathbf{p}')$ depend on both the explicit form of the chosen regulator and on the order at which one is working. Because the correction terms depend on the angles between the nucleons, they contribute to higher partial waves (nonlocal regulators only depend on the magnitudes p and p'). As a consequence, while, e.g., the LO contact interactions only describe the two S -wave channels, the use of local regulators leads to a mixing of these contributions into higher partial waves.

More generally, every regulator that respects the Fierz rearrangement freedom is an even function of \mathbf{p} and \mathbf{p}' . Then, every regulator that mixes LO physics into partial waves with odd l , e.g., P waves, and as a consequence contains terms of the form $(\mathbf{p} \cdot \mathbf{p}')^{2n+1}$, violates the Fierz rearrangement freedom. Thus, it follows that a violation of the Fierz rearrangement freedom is equivalent to a mixing of the S -wave contact interactions into odd- l partial waves. In contrast, mixing of LO contact physics into partial waves with the same S and T ($\Delta l = 2n$) is compatible with the Fierz rearrangement freedom.

Let us consider the violation of the Fierz ambiguity at LO from the point of view of a partial-wave decomposition. We again consider a Gaussian regulator in \mathbf{q} . This regulator can be rewritten as

$$\exp \left(-\frac{\mathbf{p}^2 + \mathbf{p}'^2}{\Lambda^2} \right) \exp \left(i \frac{(-2i\mathbf{p} \cdot \mathbf{p}')}{\Lambda^2} \right), \quad (12)$$

where the first factor is a typical nonlocal Gaussian regulator. The second factor, however, depends on the angle between \mathbf{p} and \mathbf{p}' . Expanding this second exponential

function in partial waves, we find

$$\exp\left(i\frac{(-2i\mathbf{p}\cdot\mathbf{p}')}{\Lambda^2}\right) = 4\pi \sum_{lm} i^l j_l \left(\frac{-2ipp'}{\Lambda^2}\right) \times Y_{lm}^*(\Omega_{p'}) Y_{lm}(\Omega_p), \quad (13)$$

with j_l a spherical Bessel function, and Y_{lm} a spherical harmonic. We can now compare the radial part for this local regulator to a nonlocal LO contact interaction with a Gaussian regulator in a partial-wave basis. The nonlocal potential leads to

$$\langle plm | V_{\text{LO}}^{\text{nonloc}}(\mathbf{p}, \mathbf{p}') | p'l'm' \rangle = 4\pi C \delta_{l0} \delta_{l'0} \delta_{m0} \delta_{m'0} \times f_R(p, p'), \quad (14)$$

while the local version takes the form

$$\langle plm | V_{\text{LO}}^{\text{loc}}(\mathbf{p}, \mathbf{p}') | p'l'm' \rangle = 4\pi C \delta_{ll'} \delta_{mm'} \times i^l j_l \left(\frac{-2ipp'}{\Lambda^2}\right) f_R(p, p') \quad (15)$$

with C a constant and $f_R(p, p') = \exp\left(\frac{-(p^2 + p'^2)}{\Lambda^2}\right)$. One can easily see that the nonlocal LO interaction in Eq. (14) only contributes for $l = l' = 0$ (S waves). The local interaction of Eq. (15), on the other hand, contributes to each partial wave with $l = l'$.

The regulator-induced contribution to all partial waves complicates fitting procedures and leads to increased theoretical uncertainties. The interaction is, however, accompanied by a Bessel function in p and p' that, for increasing orbital angular momentum l , shifts the mixed contributions to larger momenta, where they are suppressed by the regulator $f_R(p, p')$ itself. Though the preceding argument was for a specific regulator function, we expect that the violation of the Fierz rearrangement freedom has the largest effect for partial waves with small orbital angular momenta, while large- l partial waves are protected by the angular momentum barrier.

III. LOCAL CHIRAL POTENTIALS

We now investigate the impact of the violation of Fierz ambiguity on the recently developed local chiral NN potentials of Refs. [9, 10, 12, 13].

In coordinate space, the LO potential is defined by

$$V_{NN}^{\text{LO}}(r, R_L, R_S) = V_{\text{OPE}}^{\text{LO}}(r, R_L) + V_{\text{cont}}^{\text{LO}}(r, R_S), \quad (16)$$

with the long- and short-range coordinate-space cutoffs R_L and R_S , respectively. The OPE interaction has the form

$$V_{\text{OPE}}^{\text{LO}}(r, R_L) = \frac{m_\pi^3}{12\pi} \left(\frac{g_A}{2F_\pi}\right)^2 \tau_{12} \frac{e^{-m_\pi r}}{m_\pi r} \times \left[\sigma_{12} + \left(1 + \frac{3}{m_\pi r} + \frac{3}{(m_\pi r)^2}\right) S_{12} \right] f_{\text{long}}(r, R_L), \quad (17)$$

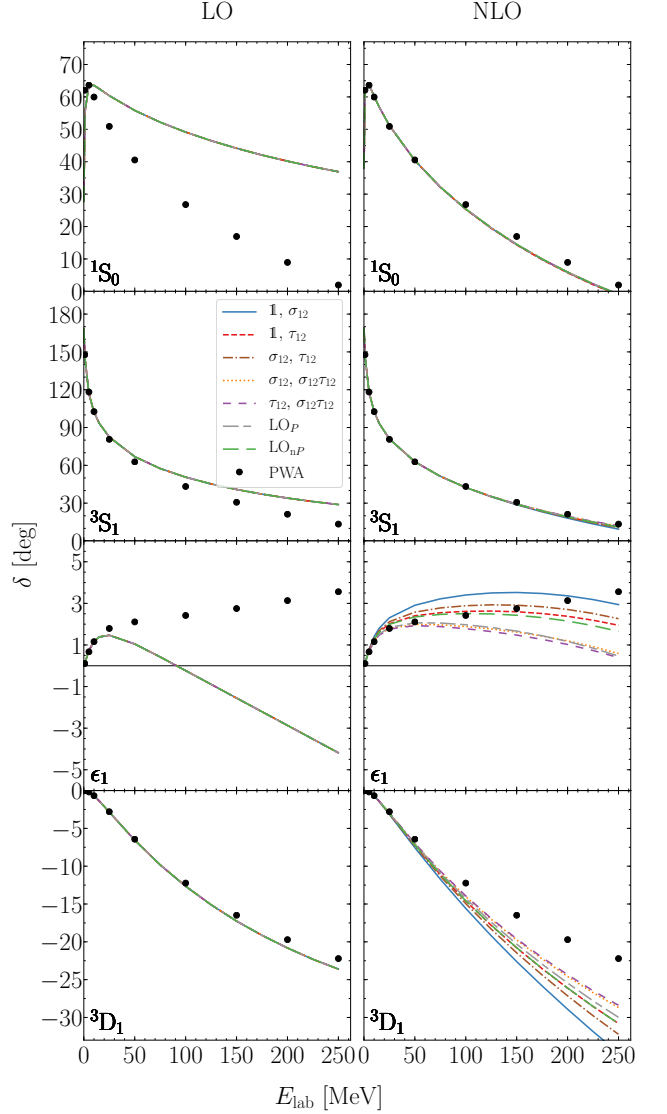


FIG. 1. Phase shifts for the 1S_0 , 3S_1 , and 3D_1 channels and the $J = 1$ mixing angle ϵ_1 for $R_0 = 1.0$ fm at LO and NLO. The S -wave phase shifts are fit and independent of the choice of the LO short-range operators. The lines for different operator choices overlap except in the case of the mixing angle ϵ_1 and the 3D_1 partial wave at NLO.

with the pion mass $m_\pi = 138.03$ MeV, the axial coupling constant $g_A = 1.29$, the pion-decay constant $F_\pi = 92.4$ MeV, and the tensor operator $S_{12} = 3\boldsymbol{\sigma}_1 \cdot \hat{\mathbf{r}} \boldsymbol{\sigma}_2 \cdot \hat{\mathbf{r}} - \sigma_{12}$. Taking the general set of momentum-independent short-range contact operators, we have

$$V_{\text{cont}}^{\text{LO}}(r, R_S) = (C_1 + C_\sigma \sigma_{12} + C_\tau \tau_{12} + C_{\sigma\tau} \sigma_{12} \tau_{12}) f_{\text{short}}(r, R_S). \quad (18)$$

Below we use the long- and short-range local regulator functions

$$f_{\text{long}}(r, R_0) = 1 - e^{-(r/R_0)^4}, \quad (19a)$$

$$f_{\text{short}}(r, R_0) = \frac{e^{-(r/R_0)^4}}{\pi\Gamma(3/4)R_0^3}, \quad (19b)$$

with a single cutoff scale $R_L = R_S = R_0$ as in Refs. [9, 10]. Our conclusions apply equally well to the long- and short-range local regulator functions of Refs. [12, 13].

If the Fierz rearrangement freedom is respected, physical observables are independent of the choice of any linearly independent set of two out of the four operators in Eq. (18). For local regulators, this is not the case and we investigate this effect by constructing LO potentials for all possible pairs of contact operators. In each case, we fit the two LECs to phase shifts in the two S -wave channels. More precisely, we fit the spin-isospin LECs to these phase shifts, which we label according to the spin and isospin quantum numbers, C_{ST} , instead of using the standard partial-wave notation, C_{2S+1L_J} . We reconstruct the operator LECs of Eq. (18) according to

$$\begin{pmatrix} C_{00} \\ C_{01} \\ C_{10} \\ C_{11} \end{pmatrix} = \begin{pmatrix} 1 & -3 & -3 & 9 \\ 1 & -3 & 1 & -3 \\ 1 & 1 & -3 & -3 \\ 1 & 1 & 1 & 1 \end{pmatrix} \begin{pmatrix} C_1 \\ C_\sigma \\ C_\tau \\ C_{\sigma\tau} \end{pmatrix}. \quad (20)$$

Note that we exclude the pair $1, \sigma_{12}\tau_{12}$ from consideration, because the operators of this pair are linearly dependent in the two S -wave channels.

We fit the LECs C_{01} and C_{10} to the 1S_0 and 3S_1 neutron-proton phase shifts from the partial-wave analysis of Ref. [29] (PWA) for cutoffs in the range $R_0 = 1.0 - 1.2$ fm. While fitting to phase shifts contains inherent drawbacks, our goal in this work is not to produce high-precision potentials. Nevertheless, we plan to fit to scattering data in future work. We use an existing automatic differentiation package [30] for Python to obtain numerical gradients for the fits, and feed these into Python's BFGS minimization routine. This algorithm is a quasi-Newton method, named after its founders Broyden, Fletcher, Goldfarb, and Shanno [31]. We perform least-square optimizations to minimize a χ^2 value with respect to the LECs. The χ^2 value is defined by

$$\chi^2 = \sum_i^{\text{data set}} \left(\frac{\delta_i^{\text{PWA}} - \delta_i^{\text{theo}}}{\Delta\delta_i} \right)^2, \quad (21)$$

where the uncertainty $\Delta\delta_i$ is given by

$$\Delta\delta_i^2 = (\Delta\delta_i^{\text{PWA}})^2 + (\Delta\delta_i^{\text{theo}})^2 + (\Delta\delta_i^{\text{num}})^2. \quad (22)$$

Here $\Delta\delta_i^{\text{PWA}}$ is the uncertainty from the PWA, $\Delta\delta_i^{\text{theo}}$ is the theoretical model uncertainty for the chiral interactions, and $\Delta\delta_i^{\text{num}}$ is due to numerical errors. For the theoretical uncertainty we use the relative uncertainty and multiply it with a constant C to obtain a dimensionless χ^2 . This is similar to the proposed uncertainty of Ref. [6]. We use $Q = \max(m_\pi, P)$, where P is a typical momentum scale of the system, and obtain for the LO and NLO uncertainties

$$\Delta\delta_i^{\text{theo,LO}} = \left(\frac{Q}{\Lambda} \right)^2 C, \quad (23)$$

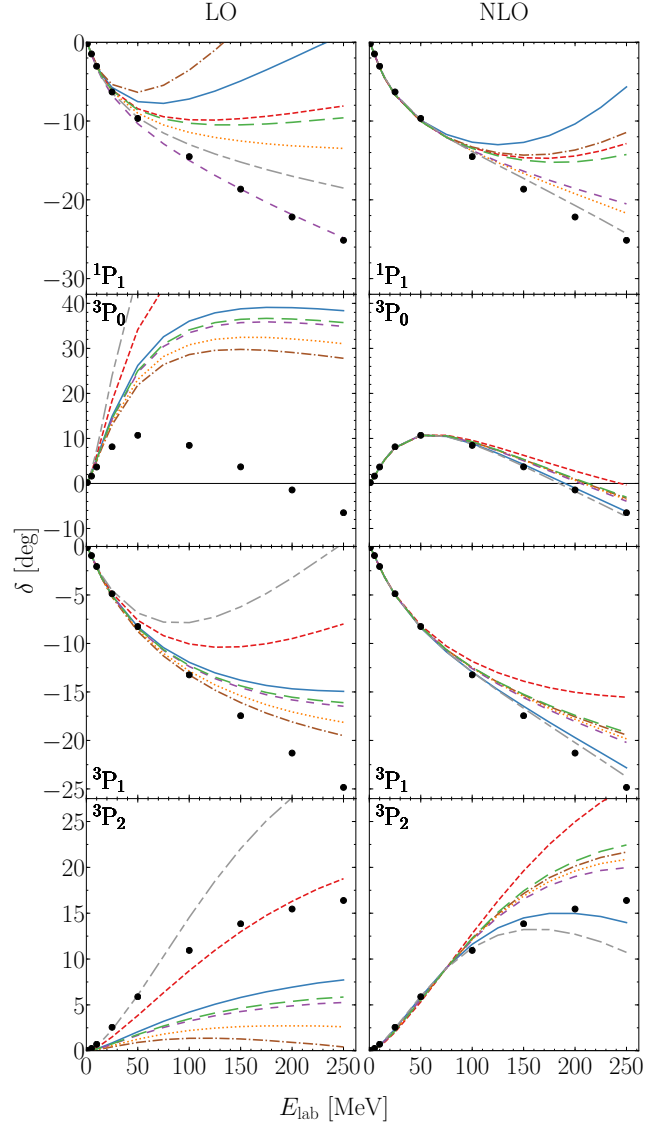


FIG. 2. Phase shifts for the 1P_1 and triplet 3P_J waves for $R_0 = 1.0$ fm. The legend is as in Fig. 1.

$$\Delta\delta_i^{\text{theo,NLO}} = \left(\frac{Q}{\Lambda} \right)^3 C, \quad (24)$$

where we take $\Lambda = 500$ MeV (400 MeV) for $R_0 = 1.0$ fm (1.2 fm) (see Ref. [20]) and $C = 1^\circ$. When studying ^4He , we choose the momentum scale associated with the average density in ^4He , $P \approx 290$ MeV, and when studying neutron matter, we choose P to be the average momentum in a Fermi gas, $P = \sqrt{3/5}k_F$, with the Fermi momentum k_F . The PWA and numerical uncertainties in $\Delta\delta_i$ are negligible compared to this theoretical model uncertainty.

We fit the interactions up to energies of 50 MeV at LO and up to 150 MeV at NLO. In particular, we fit to the energy points:

TABLE I. Operator LECs and spin-isospin LECs C_{00} and C_{11} for all investigated LO operator combinations. The cutoff R_0 is given in fm and the LEC values are given in fm². The spin-isospin LECs C_{01} (C_{10}) are -1.831 fm² (-0.317 fm²) for $R_0 = 1.0$ fm and -2.216 fm² (-1.579 fm²) for $R_0 = 1.2$ fm.

Operators	R_0	C_1	C_σ	C_τ	$C_{\sigma\tau}$	C_{00}	C_{11}
$\mathbb{1}, \sigma_{12}$	1.0	-0.696	0.378	0.000	0.000	-1.831	-0.317
	1.2	-1.738	0.159	0.000	0.000	-2.216	-1.579
$\mathbb{1}, \tau_{12}$	1.0	-1.452	0.000	-0.378	0.000	-0.317	-1.831
	1.2	-2.057	0.000	-0.159	0.000	-1.579	-2.216
σ_{12}, τ_{12}	1.0	0.000	0.726	0.348	0.000	-3.222	1.074
	1.2	0.000	1.028	0.869	0.000	-5.693	1.898
$\sigma_{12}, \sigma_{12}\tau_{12}$	1.0	0.000	0.378	0.000	0.232	0.951	0.610
	1.2	0.000	0.159	0.000	0.579	4.737	0.739
$\tau_{12}, \sigma_{12}\tau_{12}$	1.0	0.000	0.000	-0.378	0.484	5.492	0.106
	1.2	0.000	0.000	-0.159	0.686	6.649	0.526
LO_P	1.0	-1.980	-0.415	-0.793	0.101	2.548	-3.087
	1.2	-2.208	-0.346	-0.505	0.180	1.962	-2.879
LO_{nP}	1.0	-0.403	0.323	-0.055	0.134	0.000	0.000
	1.2	-0.712	0.317	0.158	0.237	0.000	0.000

TABLE II. Operator LECs for all investigated NLO operator combinations. The cutoff R_0 is given in fm and the LEC values are given in fm² for C_1, C_σ, C_τ , and, $C_{\sigma\tau}$ and in fm⁴ for $C_1 - C_7$.

Operators	R_0	C_1	C_σ	C_τ	$C_{\sigma\tau}$	C_1	C_2	C_3	C_4	C_5	C_6	C_7
$\mathbb{1}, \sigma_{12}$	1.0	2.080	1.036	0.000	0.000	0.285	0.184	-0.120	0.063	-2.241	0.304	-0.286
	1.2	0.080	0.729	0.000	0.000	0.212	0.209	-0.156	0.092	-2.112	0.343	-0.376
$\mathbb{1}, \tau_{12}$	1.0	-0.830	0.000	-0.192	0.000	0.102	-0.000	-0.149	-0.049	-1.373	0.171	-0.102
	1.2	-1.489	0.000	-0.613	0.000	-0.104	0.051	-0.298	0.035	-1.285	0.391	-0.293
σ_{12}, τ_{12}	1.0	0.000	0.296	-0.144	0.000	0.174	0.061	-0.131	-0.012	-1.698	0.205	-0.161
	1.2	0.000	0.518	-0.562	0.000	0.076	0.216	-0.255	0.139	-1.923	0.443	-0.461
$\sigma_{12}, \sigma_{12}\tau_{12}$	1.0	0.000	-0.133	0.000	0.477	0.280	-0.027	-0.109	-0.026	-1.743	0.093	-0.052
	1.2	0.000	0.054	0.000	0.651	0.381	0.028	-0.131	0.058	-2.079	0.149	-0.179
$\tau_{12}, \sigma_{12}\tau_{12}$	1.0	0.000	0.000	0.173	0.402	0.292	-0.016	-0.091	-0.036	-1.792	0.083	-0.045
	1.2	0.000	0.000	-0.071	0.681	0.373	0.023	-0.142	0.064	-2.059	0.155	-0.183
LO_P	1.0	3.517	0.409	0.414	1.246	0.562	0.053	-0.059	0.054	-2.524	0.113	-0.101
	1.2	0.843	-0.236	-0.364	1.101	0.473	0.024	-0.159	0.118	-2.201	0.168	-0.206
LO_{nP}	1.0	-0.254	0.173	-0.004	0.085	0.191	0.027	-0.116	-0.032	-1.667	0.156	-0.111
	1.2	-0.717	0.290	0.189	0.239	0.234	0.067	-0.109	-0.004	-1.927	0.170	-0.187

LO: 1, 5, 10, 25, 50 MeV,

NLO: 1, 5, 10, 25, 50, 100, 150 MeV.

For all operator pairs, we present the fitted operator LECs, as well as the spin-isospin LECs C_{00} and C_{11} in Table I and show the phase shifts at LO in the left panels of Figs. 1–3. The NLO results shown in the right panels will be discussed in Sec. V.

We begin by examining the 1S_0 , 3S_1 , and 3D_1 phase shifts as well as the $J = 1$ mixing angle in Fig. 1 for $R_0 = 1.0$ fm, in comparison to the PWA. The results for $R_0 = 1.2$ fm are qualitatively similar; see Fig. 4 for an example for the 1P_1 wave. The spin-isospin LECs C_{01} and C_{10} are fit and, thus, independent of the operator

choice. Because these LECs enter the two S -wave and the 3D_1 phase shifts, we do not observe any dependence on the operator choice. The lines for all operator pairs overlap for the 1S_0 , 3S_1 , and 3D_1 channels and the mixing angle. The obtained phase shifts are very close to the corresponding phase shifts of Ref. [10]. Furthermore, for all potentials we find the same deuteron binding energy of $E_d = 1.942$ MeV (1.949 MeV) for $R_0 = 1.0$ fm (1.2 fm).

While C_{01} and C_{10} do not depend on the chosen operator structure, it is immediately clear from Eq. (20) that the operator LECs as well as the spin-isospin LECs C_{00} and C_{11} do. When comparing the C_{00} and C_{11} values for two different operator combinations in Table I, one can

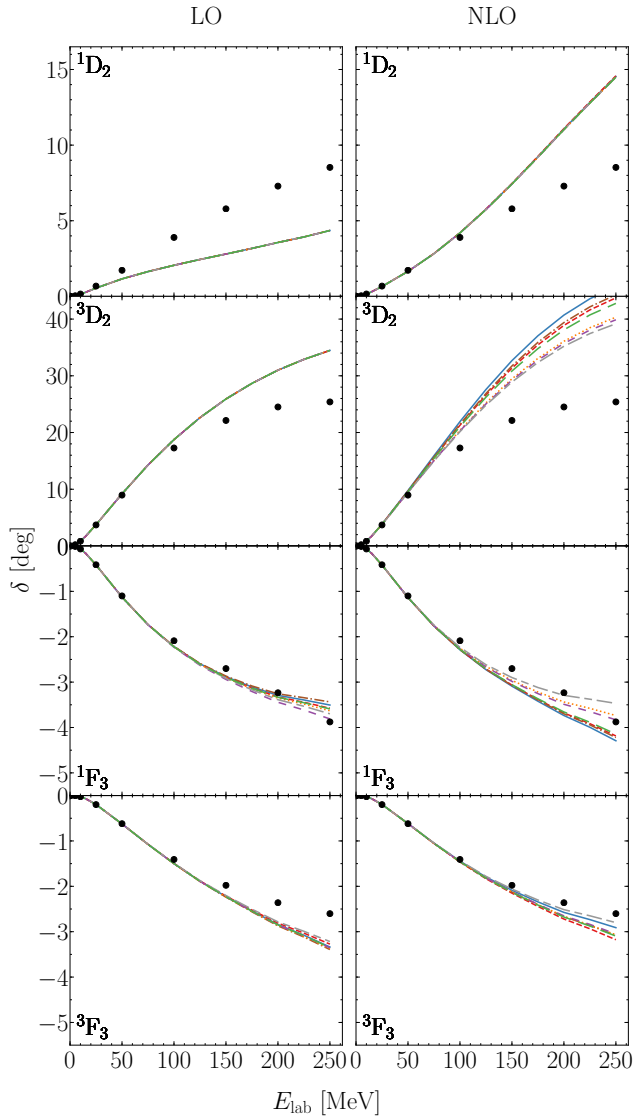


FIG. 3. Phase shifts for the 1D_2 , 3D_2 , 1F_3 , and 3F_3 partial waves for $R_0 = 1.0$ fm. The legend is as in Fig. 1.

see that the Fierz rearrangement freedom is violated for local regulators. Considering, e.g., the operator combination $\mathbb{1}, \sigma_{12}$ one obtains $C_{00} = C_{01}$ and $C_{11} = C_{10}$. For the combination $\mathbb{1}, \tau_{12}$, instead, one finds $C_{00} = C_{10}$ and $C_{11} = C_{01}$. As a consequence, the phase shifts in the corresponding spin-isospin channels are not independent of the operator choice when local regulators are used.

We show the phase shifts in the 1P_1 (determined by C_{00}) and in the 3P_J (determined by C_{11}) partial waves at LO in the upper panels of Fig. 2 for $R_0 = 1.0$ fm. At low energies, the results agree very well with the PWA, and different choices for the operator pair lead to the same phase shifts, as expected. At higher energies, however, the subleading corrections become more important and the phase shifts begin to disagree considerably with the PWA as well as with each other. For all P waves, at

energies above ≈ 20 MeV, the choice of the operator pair clearly affects the phase-shift prediction and we observe a large variation for the resulting phase shifts. This variation follows the ordering expected from Table I. In the 1P_1 partial wave, e.g., the variation ranges from results for the $\tau_{12}, \sigma_{12}\tau_{12}$ interaction, which describe the PWA results very well, to results for the σ_{12}, τ_{12} interaction that even change sign at 130 MeV.

Because the 1P_1 phase shift experiences a sizable effect, we show it again in Fig. 4 for the two operator pairs that give the extreme results and for both cutoffs. For $R_0 = 1.0$ fm, we additionally show the uncertainties according to the prescription of Ref. [3] (EKM uncertainties) at LO. We observe that the violation of the Fierz ambiguity is slightly worse for $R_0 = 1.2$ fm, which is expected based on the corresponding smaller momentum-space cutoff and, thus, larger correction terms. We also find, that the uncertainty due to the violation of the Fierz ambiguity is probed neither by varying the cutoff, which has been regarded as a tool for assessing the uncertainty due to neglecting higher-order contact operators, nor by the EKM uncertainties.

In Fig. 3 we show phase shifts for the 1D_2 , 3D_2 , 1F_3 , and 3F_3 partial waves for $R_0 = 1.0$ fm. For the D waves, only the S -wave spin-isospin LECs enter, and, thus, the LO phase shifts are independent of the short-range operators. For the F -wave phase shifts, the dependence on the short-range operator structure is nonnegligible only at energies larger than 200 MeV, because the higher- l phase shifts are protected by the angular-momentum barrier. These findings are consistent with our expectations based on the discussion around Eqs. (14) and (15).

In addition to NN scattering phase shifts, we investigate the impact of different operator choices on other physical observables. In particular, we study the ^4He ground-state energy E using the GFMC method, and the neutron-matter energy per particle E/N at different densities using the AFDMC method. The results are shown in Fig. 5 for all operator combinations, together with the corresponding EKM uncertainties as error bars. We also show the spread of all operator pairs as shaded regions. If the Fierz rearrangement freedom were respected, the spread would vanish.

For the ^4He ground-state energy, we observe a sizable dependence on the LO operator choice. The ^4He ground-state energy varies between -35.4 MeV and -44.1 MeV, the $\mathbb{1}, \tau_{12}$ interaction being an outlier due to strong P -wave attraction (excluding this operator choice, the ground-state energy only varies between -35.4 MeV and -38.8 MeV.) The spread for the different operator combinations is ~ 9 MeV and comparable to the EKM uncertainties at this order.

In the case of neutron matter, the energy per neutron at half saturation density $n_0/2$ (at n_0), with $n_0 = 0.16 \text{ fm}^{-3}$, ranges between 11.2 (16.3) MeV for the pair $\mathbb{1}, \sigma_{12}$ and 13.3 (22.1) MeV for the pair σ_{12}, τ_{12} . The spread due to the violation of Fierz rearrangement freedom is again comparable to the size of the EKM uncer-

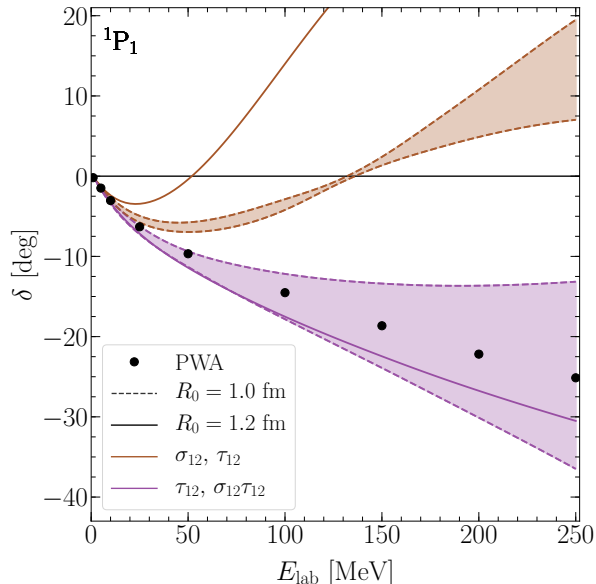


FIG. 4. Phase shift as a function of laboratory energy in the 1P_1 channel for the two interactions that give the most extreme results: the σ_{12}, τ_{12} and $\tau_{12}, \sigma_{12}\tau_{12}$ interactions. We show the results for $R_0 = 1.0$ fm with EKM uncertainty estimates (bands, see text) and the results for $R_0 = 1.2$ fm as solid lines. The color scheme is as in Fig. 1.

tainties for these interactions, which has also been observed for the leading $3N$ contact interactions [15]. Furthermore, it is important to note that the operator choice $\mathbb{1}, \tau_{12}$ leads to bound neutron matter for both densities. This can be easily understood from Table I: the spin-isospin LEC entering the triplet P waves is of the same size as the S -wave LEC and attractive for these operators. We exclude this interaction when showing the horizontal band.

IV. “COMPLETE” LO POTENTIALS

As we have seen in the previous section, the choice of the LO operators clearly impacts the results for phase shifts and the energies of nuclei and neutron matter, and leads to a range of results that is not covered by typical uncertainty estimates. To correct for this regulator artifact already at LO one could also explicitly compute the correction terms and include these in the calculation. Because it is nontrivial to include nonlocal terms in QMC simulations, we will not pursue this approach here.

Instead, we follow an idea similar to the one used in Ref. [15] and construct a LO potential with a projector on $S \neq T$ partial waves. To implement this projector, we construct a complete LO potential, i.e., a potential that includes all four LO contact operators. In addition to fitting the 1S_0 and 3S_1 phase shifts (fitting C_{01} and C_{10}),

we enforce that the contribution of $V_{\text{cont}}^{\text{LO}}(r, R_0)$ vanishes in the partial waves with $T = S$, i.e.,

$$\begin{aligned} C_{00} &= C_{\mathbb{1}} - 3C_{\sigma} - 3C_{\tau} + 9C_{\sigma\tau} = 0, \\ C_{11} &= C_{\mathbb{1}} + C_{\sigma} + C_{\tau} + C_{\sigma\tau} = 0, \end{aligned} \quad (25)$$

where we have used Eq. (20). Enforcing the two conditions in Eq. (25) eliminates the mixing into P waves. In the following, we call this interaction LO_{nP} , for “no P -wave” mixing. This potential eliminates the regulator artifacts in odd- l partial waves and, hence, is closest to an LO potential that respects the Fierz rearrangement freedom. Furthermore, it simplifies the fitting procedure for local chiral interactions at higher orders in the chiral expansion. This potential leads to a good reproduction of the P -wave phase shifts, and, for $R_0 = 1.0$ fm, gives a ^4He ground-state energy of -37.6 MeV, and a neutron-matter energy of 11.8 (17.8) MeV at $n_0/2$ (n_0). Results for this potential are also shown in Figs. 1–3 and 5.

In addition to the LO_{nP} potential, we also investigated a second complete LO potential, where we fit the additional couplings to the 1P_1 and 3P_2 partial waves. We call this interaction LO_P . In contrast to the LO_{nP} potential, the LO_P potential does not eliminate any regulator artifacts at LO but instead matches them to reproduce two P -wave phase shifts. This potential, however, is too attractive in the triplet P waves, see Table I, and performs worst in the 3P_0 and 3P_1 partial waves. We also investigated the alternatives of fitting this potential to the 1P_1 and one of the other 3P_J partial waves. These lead to an excellent description of the 3P_J wave under consideration, but an even worse reproduction of the other two triplet P waves, with, for example, $C_{11} \approx 5C_{01}$ in the fit to the 1P_1 and 3P_2 partial waves.

Due to the strong attraction in the triplet P waves, we find a large ^4He ground-state energy of ~ -51 MeV for the LO_P interaction. Furthermore, this potential leads to bound neutron matter. The LO_P potential, thus, performs worst in all systems that we studied. Again, results for this potential are shown in Figs. 1–3 and 5.

V. NEXT-TO-LEADING ORDER

As stated above, the violation of the Fierz rearrangement freedom due to the local regulator will be corrected by higher-order terms. The first correction is of the order $(Q/\Lambda)^2$ and appears at NLO in chiral EFT. In the following, we investigate to what extent the subleading NLO short-range operators restore the Fierz rearrangement freedom at LO.

At NLO, the interactions include momentum-dependent short-range contact interactions and two-pion-exchange interactions. For the contact interactions, the most general set of operators in momentum space is

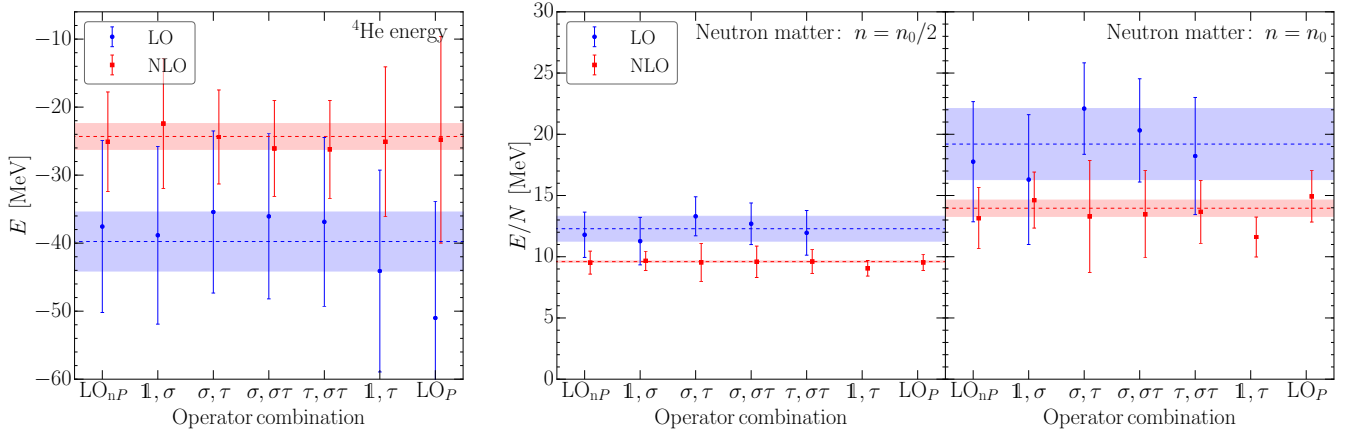


FIG. 5. Many-body observables at LO and NLO for different LO operator combinations. Here we drop the operator subscripts for legibility; i.e. $\sigma_{12} \rightarrow \sigma$, etc. The shaded regions show the spread for the various operator choices, while the dashed line denotes the centroid. When calculating the band and the centroid, we exclude the complete potentials in all cases and the $\mathbb{1}, \tau$ operator combination in the case of neutron matter. Note that for neutron matter at LO, we only show the results for five interactions, because we find bound neutron matter for the LO_P and the $\mathbb{1}, \tau_{12}$ interactions. Left panel: Ground-state energy of ${}^4\text{He}$. Middle panel: Neutron matter energy per particle at one half saturation density. Right panel: Neutron matter energy per particle at saturation density.

given by 14 different terms,

$$\begin{aligned}
 V_{\text{cont}}^{(2)} = & \gamma_1 q^2 + \gamma_2 q^2 \sigma_{12} + \gamma_3 q^2 \tau_{12} + \gamma_4 q^2 \sigma_{12} \tau_{12} \\
 & + \gamma_5 k^2 + \gamma_6 k^2 \sigma_{12} + \gamma_7 k^2 \tau_{12} + \gamma_8 k^2 \sigma_{12} \tau_{12} \\
 & + \gamma_9 (\boldsymbol{\sigma}_1 + \boldsymbol{\sigma}_2) \cdot (\mathbf{q} \times \mathbf{k}) + \gamma_{10} (\boldsymbol{\sigma}_1 + \boldsymbol{\sigma}_2) \cdot (\mathbf{q} \times \mathbf{k}) \tau_{12} \\
 & + \gamma_{11} (\boldsymbol{\sigma}_1 \cdot \mathbf{q})(\boldsymbol{\sigma}_2 \cdot \mathbf{q}) + \gamma_{12} (\boldsymbol{\sigma}_1 \cdot \mathbf{q})(\boldsymbol{\sigma}_2 \cdot \mathbf{q}) \tau_{12} \\
 & + \gamma_{13} (\boldsymbol{\sigma}_1 \cdot \mathbf{k})(\boldsymbol{\sigma}_2 \cdot \mathbf{k}) + \gamma_{14} (\boldsymbol{\sigma}_1 \cdot \mathbf{k})(\boldsymbol{\sigma}_2 \cdot \mathbf{k}) \tau_{12}.
 \end{aligned} \quad (26)$$

As before, only seven out of these 14 operators are independent for reasons of antisymmetry if no regulator is included. We use the same local regulators at NLO as we did at LO. Then, the Fierz rearrangement freedom is again violated at NLO. In the following, however, we neglect the new regulator artifacts that originate at NLO and instead focus only on the LO regulator artifacts because they are the largest in size: The corrections to the NLO violation appear only at N^3LO . Furthermore, the NLO regulator artifacts in S and P waves can be absorbed into the LECs and the first artifacts then appear in D waves, where they are additionally suppressed by the angular momentum barrier.

In the following, we construct NLO interactions for all possible pairs of LO operators, as well as the two potentials with the complete set of LO operators (LO_{nP} and LO_P). We fix the NLO operators to be the six local operators and the spin-orbit operator, as in Refs. [9, 10]: $\{\mathbb{1}, \sigma_{12}, \tau_{12}, \sigma_{12}\tau_{12}, (\boldsymbol{\sigma}_1 \cdot \mathbf{q})(\boldsymbol{\sigma}_2 \cdot \mathbf{q}), (\boldsymbol{\sigma}_1 \cdot \mathbf{q})(\boldsymbol{\sigma}_2 \cdot \mathbf{q})\tau_{12}\}$ and $(\boldsymbol{\sigma}_1 + \boldsymbol{\sigma}_2) \cdot (\mathbf{q} \times \mathbf{k})$.

In addition to the S -wave phase shifts, we fit the LECs to the $J = 1$ mixing angle ϵ_1 and the 1P_1 and 3P_J partial waves. We give the NLO LECs for all interactions in Table II.

We present the NLO phase shifts in the right panels

in Figs. 1–3. Regarding the S -wave phase shifts, we find a good description of the PWA results. Again, all seven interactions produce the same phase shifts. In the coupled channel, for the $J = 1$ mixing angle and the 3D_1 phase shift, we observe a dependence on the operator choice. The reason is that the LECs describing the NLO tensor-contact interactions are different for all operator pairs in order to reproduce the P -wave phase shifts. The different tensor interactions then lead to differences in the 3D_1 coupled channel, which affects the mixing angle. For the deuteron binding energy, we find an (almost) operator independent result of $E_d = 2.113 - 2.134$ (2.107 – 2.162) MeV for $R_0 = 1.0$ fm (1.2 fm), where the range is again due to the somewhat different tensor interactions.

Turning to the P waves in Fig. 2, we observe two effects at NLO. First, the reproduction of the PWA values is much better for both the singlet and triplet partial waves. Second, we find that the effects of the violation of the Fierz rearrangement freedom are considerably reduced. At LO, we found a sizable spread of the description of the P -wave phase shifts already at energies around 20 MeV. At NLO, all interactions lead to similar phase shifts up to energies of ~ 100 MeV, but sizable regulator artifacts remain at higher laboratory energies. The impact of the violation of the Fierz ambiguity is worst in the 3P_2 wave where the spin-orbit interaction is attractive and the tensor is weakest. Finally, for the higher- l partial waves in Fig. 3, we find similar results for the phase shifts as at LO: These phase shifts are already well described by the OPE interaction at LO and improvements with the chiral order are counteracted by the different tensor interactions. However, the violation of the Fierz rearrangement freedom has only a small impact on these partial waves.

We now discuss the effects on the many-body observables. For the ${}^4\text{He}$ ground-state energy we find that the spread for different LO operator pairs reduces considerably: from 8.7 MeV at LO to 3.8 MeV at NLO, ranging from 22.4 MeV for the $\mathbb{1}, \sigma_{12}$ interaction to 26.2 MeV for the $\tau_{12}, \sigma_{12}\tau_{12}$ interaction. The spread is considerably smaller than the EKM uncertainties of at least 7 MeV, in contrast to the results at LO.

We show the neutron-matter energy at $n_0/2$ in the middle panel of Fig. 5. In contrast to the results at LO, we now find all interactions produce unbound neutron matter at roughly the same energy in the range of 9.1–9.7 MeV. Thus, for neutron matter at $n_0/2$ the Fierz ambiguity is almost completely restored and the uncertainty from choosing different operator pairs is smaller than the EKM uncertainties. At higher density, n_0 , the spread between different interactions remains larger at 3.0 MeV, ranging from 11.6 MeV for the $\mathbb{1}, \sigma_{12}$ interaction up to 14.6 MeV for the $\mathbb{1}, \sigma_{12}$ interaction; see the right panel of Fig. 5. This is to be expected, as the regulator artifacts increase with momentum or density (see also Refs. [11, 21]).

Considering only the interactions that gave reasonable results already at LO, the spread reduces to 1.5 MeV and is, thus, only 1/4 of the spread at LO (5.8 MeV) and smaller than the EKM uncertainties of ≈ 2 MeV. The ordering of the NLO results closely follows the ordering of the description of the triplet P waves, with the $\mathbb{1}, \tau_{12}$ interaction being the biggest outlier.

In summary, we find that the violation of the Fierz ambiguity in the NN sector is considerably reduced at NLO, and always covered by the EKM uncertainties, in contrast to the results at LO. The violation of the Fierz ambiguity will remain of similar size at $N^2\text{LO}$ because no new contact terms are introduced, but we expect that it should be almost completely removed at $N^3\text{LO}$. As a consequence of these findings, recently derived local NN potentials at $N^2\text{LO}$ can be used with confidence within their uncertainties.

Finally, we discuss implications for $3N$ interactions. We found that the spread induced by different operator choices is sizable for the leading NN interactions. This is also the case for the leading $3N$ interactions as shown in Refs. [15, 21]. Our results demonstrate that the subleading contact interactions are necessary to reduce this spread. While in the NN sector they appear already at NLO in chiral power counting, the subleading $3N$ contact interactions only enter at $N^4\text{LO}$. The implementation of the $N^4\text{LO}$ $3N$ forces is certainly challenging. Therefore, in order to tackle the violation of Fierz rearrangement freedom in the $3N$ sector, other ideas are necessary. These include the choice of the projected V_E interaction of Ref. [15] or increasing the (momentum-space) cutoff for chiral interactions. However, we also note that we expect the EKM uncertainties to cover this effect for many (but not all) nuclear systems. In particular, for nuclear systems with densities (momenta) of the order of saturation density, we expect the EKM uncertainties to

underestimate the effect coming from the violation of the Fierz ambiguity.

VI. CONCLUSION AND OUTLOOK

In summary, we investigated the violation of the Fierz rearrangement freedom that appears when using local regulators in the NN sector at LO in chiral EFT. We constructed interactions at LO and NLO in chiral EFT for all possible pairs of LO operators where we fitted the LECs to the PWA results for the two S -wave phase-shift channels. We also constructed two complete LO interactions where we determined the additional two LECs either by projecting on partial waves with $S = T$ (attempting to restore the Fierz rearrangement freedom), or by fitting to the 1P_1 and 3P_2 phase shifts.

We studied phase shifts, the deuteron and ${}^4\text{He}$ binding energies, as well as the energy of neutron matter at different densities for all of these interactions. Because we fitted the LECs to the two $S \neq T$ channels, we found that all interactions lead to a similar description for these channels at LO. For the $S = T$ channels, i.e., the 1P_1 and 3P_J partial waves, we found instead a strong dependence on the chosen operator structure for energies of the order of 20 MeV. At NLO, in addition to an improved description of the phase shifts in general, we found the effect of the violation of the Fierz rearrangement freedom to be reduced considerably, having an effect only at energies larger than 100 MeV.

We then studied the ${}^4\text{He}$ ground-state energy, where the uncertainty due to the violation of the Fierz ambiguity reduced considerably when going from LO to NLO, from 8.7 MeV to 3.8 MeV. In neutron matter, we found a sizable dependence on the chosen operator structure at LO. In particular, two interactions lead to bound neutron matter. For the five interactions that did not show a collapse, the spread from choosing different operator pairs reduced from 2.0 (5.8) MeV to 0.2 (1.5) MeV when going from LO to NLO for $n = n_0/2$ (n_0). At NLO, we found this spread to be much smaller than the EKM uncertainties for both densities. Furthermore, at saturation density, the operator dependence for the leading NN interactions was found to be smaller than that for the leading $3N$ forces at $N^2\text{LO}$, with the latter being ≈ 4 MeV for the three different operator choices in Ref. [15].

We found that the violation of the Fierz ambiguity in the NN sector is sizable at LO but restored to a large extent by including the subleading contact operators at NLO. Any remaining violations of the Fierz ambiguity at higher orders in the NN sector are significantly smaller than the violation from the leading $3N$ interaction at $N^2\text{LO}$. The situation will further improve when contact interactions at $N^3\text{LO}$ are included because additional correction terms will absorb the remaining regulator artifacts. Local chiral NN interactions, thus, can be used with confidence even though additional regulator artifacts appear.

ACKNOWLEDGMENTS

We thank S. Gandolfi for useful discussions. L.H. thanks the Institute for Nuclear Theory in Seattle for its hospitality. This work was supported by the ERC Grant No. 307986 STRONGINT, the National Science Foundation Grant No. PHY-1430152 (JINA-CEE), the

U.S. DOE under Grant No. DE-FG02-00ER41132, and the NUCLEI SciDAC program. Computational resources have been provided by the Jülich Supercomputing Center, and the Lichtenberg high performance computer of the TU Darmstadt. We also used resources provided by NERSC, which is supported by the U.S. DOE under Contract No. DE-AC02-05CH11231.

-
- [1] E. Epelbaum, H.-W. Hammer, and U.-G. Meißner, *Rev. Mod. Phys.* **81**, 1773 (2009).
 - [2] R. Machleidt and D. R. Entem, *Phys. Rep.* **503**, 1 (2011).
 - [3] E. Epelbaum, H. Krebs, and U.-G. Meißner, *Eur. Phys. J. A* **51**, 53 (2015).
 - [4] E. Epelbaum, H. Krebs, and U. G. Meißner, *Phys. Rev. Lett.* **115**, 122301 (2015).
 - [5] A. Ekström, G. R. Jansen, K. A. Wendt, G. Hagen, T. Papenbrock, B. D. Carlsson, C. Forssén, M. Hjorth-Jensen, P. Navrátil, and W. Nazarewicz, *Phys. Rev. C* **91**, 051301 (2015).
 - [6] B. D. Carlsson, A. Ekström, C. Forssén, D. F. Strömberg, G. R. Jansen, O. Lilja, M. Lindby, B. A. Mattsson, and K. A. Wendt, *Phys. Rev. X* **6**, 011019 (2016).
 - [7] D. R. Entem, R. Machleidt, and Y. Nosyk, *Phys. Rev. C* **96**, 024004 (2017).
 - [8] M. Fierz, *Z. Phys* **104**, 553 (1937).
 - [9] A. Gezerlis, I. Tews, E. Epelbaum, S. Gandolfi, K. Hebeler, A. Nogga, and A. Schwenk, *Phys. Rev. Lett.* **111**, 032501 (2013).
 - [10] A. Gezerlis, I. Tews, E. Epelbaum, M. Freunek, S. Gandolfi, K. Hebeler, A. Nogga, and A. Schwenk, *Phys. Rev. C* **90**, 054323 (2014).
 - [11] I. Tews, S. Gandolfi, A. Gezerlis, and A. Schwenk, *Phys. Rev. C* **93**, 024305 (2016).
 - [12] M. Piarulli, L. Girlanda, R. Schiavilla, R. N. Pérez, J. E. Amaro, and E. R. Arriola, *Phys. Rev. C* **91**, 024003 (2015).
 - [13] M. Piarulli, A. Baroni, L. Girlanda, A. Kievsky, A. Lovato, E. Lusk, L. E. Marcucci, S. C. Pieper, R. Schiavilla, M. Viviani, and R. B. Wiringa, [arXiv:1707.02883](https://arxiv.org/abs/1707.02883).
 - [14] J. E. Lynn, J. Carlson, E. Epelbaum, S. Gandolfi, A. Gezerlis, and A. Schwenk, *Phys. Rev. Lett.* **113**, 192501 (2014).
 - [15] J. E. Lynn, I. Tews, J. Carlson, S. Gandolfi, A. Gezerlis, K. E. Schmidt, and A. Schwenk, *Phys. Rev. Lett.* **116**, 062501 (2016).
 - [16] P. Klos, J. E. Lynn, I. Tews, S. Gandolfi, A. Gezerlis, H.-W. Hammer, M. Hoferichter, and A. Schwenk, *Phys. Rev. C* **94**, 054005 (2016).
 - [17] J.-W. Chen, W. Detmold, J. E. Lynn, and A. Schwenk, [arXiv:1607.03065](https://arxiv.org/abs/1607.03065).
 - [18] M. Piarulli, L. Girlanda, R. Schiavilla, A. Kievsky, A. Lovato, L. E. Marcucci, S. C. Pieper, M. Viviani, and R. B. Wiringa, *Phys. Rev. C* **94**, 054007 (2016).
 - [19] S. Gandolfi, H.-W. Hammer, P. Klos, J. E. Lynn, and A. Schwenk, *Phys. Rev. Lett.* **118**, 232501 (2017).
 - [20] J. E. Lynn, I. Tews, J. Carlson, S. Gandolfi, A. Gezerlis, K. E. Schmidt, and A. Schwenk, [arXiv:1706.07668](https://arxiv.org/abs/1706.07668).
 - [21] A. Dyhdalo, R. J. Furnstahl, K. Hebeler, and I. Tews, *Phys. Rev. C* **94**, 034001 (2016).
 - [22] A. Lovato, O. Benhar, S. Fantoni, and K. E. Schmidt, *Phys. Rev. C* **85**, 024003 (2012).
 - [23] P. Navrátil, *Few Body Syst.* **41**, 117 (2007).
 - [24] U. van Kolck, *Phys. Rev. C* **49**, 2932 (1994).
 - [25] E. Epelbaum, A. Nogga, W. Glöckle, H. Kamada, U.-G. Meißner, and H. Witała, *Phys. Rev. C* **66**, 064001 (2002).
 - [26] J. Carlson, S. Gandolfi, F. Pederiva, S. C. Pieper, R. Schiavilla, K. E. Schmidt, and R. B. Wiringa, *Rev. Mod. Phys.* **87**, 1067 (2015).
 - [27] D. R. Entem and R. Machleidt, *Phys. Rev. C* **68**, 041001 (2003).
 - [28] E. Epelbaum, W. Glöckle, and U.-G. Meißner, *Nucl. Phys. A* **747**, 362 (2005).
 - [29] V. G. J. Stoks, R. A. M. Klomp, M. C. M. Rentmeester, and J. J. de Swart, *Phys. Rev. C* **48**, 792 (1993).
 - [30] A. D. Lee, “A Python package for first- and second-order automatic differentiation,” <http://pythonhosted.org/ad/>.
 - [31] J. Nocedal and S. J. Wright, *Numerical Optimization*, 2nd ed. (Springer, New York, 2006) p. 136.